Localized surface Plasmon Bragg grating on SOI waveguide at telecom wavelengths

M. Fevrier[1,2], P. Gogol[1,2], A. Aassime[1,2], R. Mégy[1,2], D. Bouville[1,2], J. M. Lourtioz[1,2] and B. Dagens[1,2*]
1. Univ Paris-Sud, Laboratoire IEF, UMR 8622, Orsay, F-91405, France
2. CNRS, Orsay, F-91405, France
[*]corresponding author: beatrice.dagens@ief.u-psud.fr

Abstract

We show that the metal nanoparticle chains supporting localized surface plasmon resonance can behave as transmission Bragg gratings on a dielectric waveguide. An analytical model is developed to interpret the experimental results.

1. Introduction

Metallic nanoparticles (MNP) supporting localized surface plasmons (LSPs) can confine light at sub-wavelength scales [1] with many potential applications in plasmonic nanolasers [2], SERS [3,4], bio-sensors [5], waveguiding [6] – [8]. To date, most of the studies conducted on the LSPs have been performed using free-space or near-field configurations, where MNP chains can incidentally behave as grating couplers. For instance, an increase in the LSP resonance lifetime was demonstrated by using a diffraction order of a MNP [9] – [11]. In 2004, Quidant *et al.* observed strong modulations in the near-field spectra of a composite device including MNPs with TiO_2 microguide at visible frequency [12]. Recently Zhou *et al.* reported polariton propagation in a 2D grating of gold NPs by coupling either to the transverse or longitudinal resonant LSP modes [13]. Yet, the excitation of LSP in a truly guided configuration remains a crucial step towards the implementation of plasmonic functions in photonic integrated circuits.

In this paper, we analyze both theoretically and experimentally the LSP Bragg grating (LSPBG) integrated in a guided wave SOI (silicon-on-insulator) configuration at telecom wavelengths. We show that different propagation regimes and transmission spectra at the waveguide output can be obtained depending on the position of Bragg frequency orders with respect to the LSP resonance. To investigate theoretically the behavior of such LSPBGs, we propose an analytical model where the MNP is described as a periodic modulation of the waveguide refractive index. Prior to this, an equivalent index of the metallic film is derived from the coupled dipole approximation method in the quasi-static approximation. Our approach is similar to that recently used for modeling the optical properties of 2D gold NP grating excited in Kretshman-Raether configuration [14]. The propagation in the waveguide with LSP Bragg grating is then described by using the coupled mode theory (CMT) [15-16].

The paper is organized as follows. The analytical model of LSPBG is presented in the next section. The different LSPBG behaviors are then illustrated by varying the LSP resonance frequency (i.e., the size of nanoparticles) at a constant grating period. Next, Finite Difference Time Domain (FDTD) calculations are used to validate the main assumptions in the model. Experiments are then presented, and waveguide transmission measurements are compared to theoretical predictions.

2. Analytical model of LSP Bragg gratings

Fig. 1(a) show the basic scheme of a dielectric (SOI) waveguide with a LSP Bragg grating deposited on the top. The inter-particle distance d is chosen to provide at least one grating order within the wavelength range of interest. The size of the nanoparticles is chosen in such a way that the LSP resonance occur in the same wavelength range. One appropriate shape to excite the LSP resonance with a TE waveguide mode is the ellipsoidal nanorod with its long axis perpendicular to the mode of propagation (fig. 1 (b)). In what follows, D1 and D2 will denote the long axis and small axis respectively. As gold is an absorbing material, MNPs can actually perturb the waveguide's refractive index in two ways. They not only affect the real part of the refractive index, but also its imaginary part. As will be seen later, this can lead to different LSPBG regimes depending on the respective positions of Bragg and LSP resonances.

Coupled mode theory is commonly used to provide an analytical description of Bragg gratings [17]. However, LSPBG is not a standard case since both the LSP resonance and the Bragg resonance must be accounted for. Here, we make the assumption that an equivalent index of refraction $\tilde{n}_{eq}$ can be assigned to the MNP grating layer supporting LSP resonance. To calculate $\tilde{n}_{eq}$ each MNP is approximated by a point dipole, and its interaction with the underlying waveguide is accounted for via the image dipole formalism. The quasi-static approximation is then used since the inter-particle spacing (~ 500 nm) is sufficiently long to assume uncoupled particles. The same approach was made for 2D grating of MNPs excited in the Kretshman-Raether configuration [14] as well as for a Bragg grating in a free space configuration [18]. The originality of our approach stems from the use of a waveguide configuration. Once

$\tilde{n}_{eq}$ is obtained, it is injected in the CMT model to calculate the waveguide transmission (Figure1 (c)).

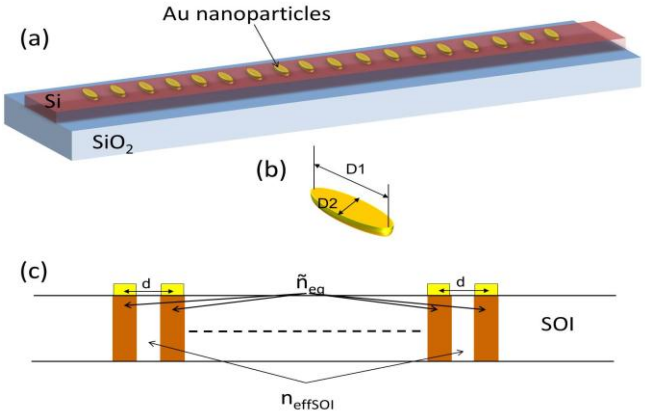

Figure 1: (a) Schematic view of a LSP Bragg grating on SOI waveguide. (b) Schematic view of a given nanoparticle. (c) Principle scheme for the analytical model. Nanoparticles are replaced by transverse waveguide slices with an equivalent index $\tilde{n}_{eq}$.

2.1. Determination of the equivalent index layer

We consider a MNP grating on a substrate with a permittivity ε_{sub} and immerged in a medium having permittivity ε_{ext}. The MNP grating layer is presently approximated by an equivalent medium with a dielectric function ε_{eq}. The term "equivalent" is preferred to "effective" in order not to be confused with the effective index of the waveguide. The macroscopic polarization $\vec{P}$ of this equivalent medium is then related to its permittivity and the macroscopic external field $\vec{E}_{ext}$ via [19]:

$$\vec{P} = \varepsilon_0(\varepsilon_{eq} - \varepsilon_{ext})\vec{E}_{ext}, \quad (1)$$

The polarization $\vec{P}$ is also written as the sum of the dipolar moments $\vec{p}$ of individual particles $\vec{P} = N\vec{p}$ where N is the number of particles per unit volume. This lead to:

$$\vec{P} = N\varepsilon_0 V\alpha(\omega)\varepsilon_{ext}\vec{E}_{loc}, \quad (2)$$

where V is the volume and α(ω) is the polarisability of an individual particle $\vec{E}_{loc}$ is the local field "seen" by this particle. In the quasi-static approximation, the polarisability of an ellipsoidal particle with permittivity ε_m and a depolarization factor L_s in a medium with permittivity ε_{ext} is defined by [20] :

$$\alpha(\omega) = \frac{\varepsilon_m - \varepsilon_{ext}}{\varepsilon_{ext} + L_s(\varepsilon_m - \varepsilon_{ext})}, \quad (3)$$

When the local field $\vec{E}_{loc}$ is known, it is possible to determine the equivalent permittivity ε_{eq} from equation (1) and (2):

$$\varepsilon_0(\varepsilon_{eq} - \varepsilon_{ext})\vec{E}_{ext} = N\varepsilon_0 V\alpha(\omega)\varepsilon_{ext}\vec{E}_{loc}. \quad (4)$$

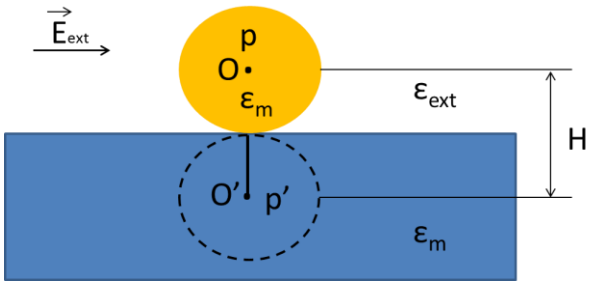

Figure 2: Schematic of a particle placed on a substrate and its image dipole.

Actually, $\vec{E}_{loc}$ can be calculated by considering the particle as a point dipole. The image dipole formalism is then used to account for the presence of a substrate that is presently assumed to be isotropic and non-magnetic (fig. 2). The image dipole $\vec{p}'$ associated with the dipole moment $\vec{p}$ carried by the particle at the interface between the substrate (ε_{sub}=3.59) and the external medium (ε_{ext}=1), is written [21]:

$$\vec{p}' = -\vec{p}\frac{\varepsilon_{sub} - \varepsilon_{ext}}{\varepsilon_{ext} + \varepsilon_{sub}}. \quad (5)$$

The local field in O then results from two contributions, the applied external field $\vec{E}_{ext}$ and the field created by the image dipole $\vec{E}_{img}$: $\vec{E}_{loc} = \vec{E}_{ext} + \vec{E}_{img}$. The electrostatic potential created at any point in space is the sum of the potentials created by dipole $\vec{p}$ and image dipole $\vec{p}'$, respectively. Using the quasi-static approximation, the general expression of the field created by a dipole $\vec{p}$ at a distance r (point M) in a medium with a dielectric ε_{ext} is given by the following equation:

$$\vec{E}_{dip} = \frac{1}{4\pi\varepsilon_0\varepsilon_{ext}}\frac{3(\vec{p}.\vec{R})\vec{R} - \vec{p}}{r^3}, \quad (6)$$

where $\vec{R} = r.\vec{u}$, $\vec{u}$ is the unit vector born by $\overrightarrow{OM}$. Using the general expression (6), the field created by the image dipole $\vec{p}'$ located in O' at point O is given by:

$$\vec{E}_{dip} = \frac{1}{4\pi\varepsilon_0\varepsilon_{ext}}\frac{3(\vec{p}'.\overrightarrow{O'O})\overrightarrow{O'O} - \vec{p}'}{\left|\overrightarrow{O'O}\right|^3}, \quad (7)$$

Since the image dipole $\vec{p}'$ is oriented perpendicularly to $\overrightarrow{O'O}$, then: $\vec{p}'.\overrightarrow{O'O} = 0$. By denoting $\left|\overrightarrow{O'O}\right| = H$ and using Eq. (5), the expression for the field $\vec{E}_{img}$ can be re-written as:

$$\vec{E}_{img} = -\frac{1}{4\pi\varepsilon_0\varepsilon_{ext}}\frac{\vec{p}'}{r^3} = \frac{1}{4\pi\varepsilon_0\varepsilon_{ext}H^3}\frac{\varepsilon_{sub}-\varepsilon_{ext}}{\varepsilon_{ext}+\varepsilon_{sub}}\vec{p} \qquad (8)$$

This leads to the following expression $\vec{E}_{loc}$:

$$\vec{E}_{loc} = \frac{1}{4\pi\varepsilon_0\varepsilon_{ext}}\left(\frac{\varepsilon_{sub}-\varepsilon_{ext}}{\varepsilon_{ext}+\varepsilon_{sub}}\frac{\vec{p}}{H^3}\right)+\vec{E}_{ext} \qquad (9)$$

where $\vec{P} = N\varepsilon_0 V\alpha(\omega)\varepsilon_{ext}\vec{E}_{loc}$. Let us define K as:

$$-K = \frac{1}{4\pi\varepsilon_0\varepsilon_{ext}}\left(\frac{\varepsilon_{sub}-\varepsilon_{ext}}{\varepsilon_{ext}+\varepsilon_{sub}}\frac{1}{H^3}\right). \qquad (10)$$

The equivalent permittivity ε_{eq} is then determined by using the eqs. (4), (9) and (10). After straightforward calculations, we obtain:

$$\varepsilon_{eq} = \varepsilon_{ext} + \frac{NV\alpha(\omega)\varepsilon_{ext}}{1+KV\varepsilon_0\varepsilon_{ext}\alpha(\omega)}. \qquad (11)$$

The expression for ε_{eq} (or rather, that of $\tilde{n}_{eq} = \sqrt{\varepsilon_{eq}}$) is then used in the coupled mode theory to account for the LSP resonance in the Bragg grating. Here it is worthwhile recalling that the "one-particle" model used to derive ε_{eq} not only assumes uncoupled particles, but also neglects radiation losses in the system. As will be seen in Section 5, this leads to a non-symmetric plasmon absorption line whose width is narrower thanthe measured line widths. In turn, basic mechanisms of LSP Bragg grating are correctly described.

2.2. Coupled mode theory with LSP resonance

In order to adapt CMT [17] to LSP Bragg gratings, we use the simplified scheme of a periodically structured waveguide shown in fig. 1(c). In waveguide regions close to the particles, the waveguide refractive index is taken to be equal to $\tilde{n}_{eq}$. In other regions, the effective index of the bare waveguide, $n_{eff_{SOI}}$ = 2.32 is maintained. This implicitly assumes that in the waveguide regions close to the particles, the electromagnetic energy of the TE guided mode is almost totally transferred to the particles themselves. FDTD simulations reported in Section 4 supports this assumption.

The periodic modulation thus simulated along the waveguide simultaneously includes a "pure" refractive index modulation (real part of the index) and a loss modulation due to nanoparticles (imaginary part of the index). Using the general expression of complex refractive index for a material having a gain (or loss), $\tilde{n}_{eq}$ is written as:

$$\tilde{n}_{eq} = n_{eq} + i\frac{\gamma_{eq}}{k_0} \qquad (12)$$

where $k_0=2\pi/\lambda$, λ is the wavelength, n_{eq} the refractive index and γ_{eq} the material gain (or losses if $\gamma < 0$) which is constant in intensity. For the sake of simplicity, we consider a sinusoidal modulation along the waveguide with real part oscillating between n_{effsoi} and n_{eq} and the imaginary part oscillating between 0 and γ_{eq}/k_0. For such a modulation, the spatial evolutions of the real and imaginary parts of the optical index in the propagation direction equal:

$$n(x) = n_0 + n_1\cos\left(\frac{2\pi x}{d}\right) \qquad (13)$$
$$\gamma(x) = \gamma_0 + \gamma_1\cos\left(\frac{2\pi x}{d}\right)$$

where the value of n_0, n_1, γ_0 and γ_1 are determined from the initial conditions. Setting the origin at the first particle, we obtain:

$$n_0 = \frac{n_{eq}-n_{eff_{SOI}}}{2}$$
$$n_1 = \frac{n_{eq}+n_{eff_{SOI}}}{2} \qquad (14)$$
$$\frac{\gamma_0}{k_0} = \frac{\gamma_1}{k_0}$$
$$\frac{\gamma_1}{k_0} = \frac{\gamma_{eq}}{2k_0}$$

The CMT model then leads to the following coupled differential system [17]:

$$\frac{dA}{dx} = -i\kappa B(x)e^{i2\Delta\beta x} + i\gamma_0 A(x) \qquad (15)$$
$$\frac{dB}{dx} = i\kappa A(x)e^{-i2\Delta\beta x} - i\gamma_0 B(x)$$

where A(x) and B(x) represent the propagative and contra-propagative modes, respectively. The coupling constant, κ, is given by:

$$\kappa = \frac{\pi}{\lambda_0}\left(\frac{n_{eq}+n_{eff_{SOI}}}{2}+i\frac{\gamma_{eq}}{2k_0}\right). \qquad (16)$$

The phase mismatch 2β is given by:

$$2\Delta\beta = n_{eff_{SOI}}\frac{2\pi}{\lambda} - m\frac{2\pi}{d}. \qquad (17)$$

The resolution of coupled differential equations (15) allows us to calculate the normalized transmission and reflection coefficients for the waveguide with LSP Bragg grating:

$$T = \left\|\frac{A(x)}{A_0}\right\|^2. \qquad (18)$$
$$R = \left\|\frac{B(x)}{A_0}\right\|^2$$

Let us recall here that the specific parameters of nanoparticles are included in the model via Eq. (3). In what

follows, the particle size is used as a variable parameter to investigate the different behaviors of LSP Bragg grating.

3. LSP Bragg grating behaviors

We consider a Bragg grating made of 50 particles with the Bragg resonance at λ=1500 nm. In principle, particles should be spaced 300 nm apart in order to operate in the first Bragg order. However, this would lead in turn to strong coupling between particles with the consequences that MNP chain itself would behave as a waveguide [8] and the Bragg grating mechanism would be strongly perturbed. For this reason, a 600 nm spacing is fixed between particles corresponding to a second-order grating. Fig. 3 shows the calculated waveguide transmission and reflection for LSP Bragg gratings with different MNP sizes. Three situations are found depending on the spectral position of the LSP. If the LSP resonance occurs at a shorter wavelength than the Bragg resonance (fig. 3(a)), the waveguide transmission exhibits a minimum at the Bragg wavelength as expected. In case the LSP resonance coincides with the Bragg resonance, the transmission dip is replaced by a small transmission peak. At the same time, the Bragg reflection is significantly attenuated (fig. 3(b)). When the plasmon resonance wavelength is longer than the Bragg wavelength λ_{Bragg}, a weak but quite detectable peak appears in the transmission spectrum (fig. 3(c)). Calculated curves showing the real (n_{eq}) and imaginary ($k_{eq}=\gamma_{eq}/k_0$) parts of the equivalent layer index (right column in fig. 3) help us to explain the different behaviors. For a plasmon resonance at short wavelength (fig. 3(a)), the real part of the refractive index dominates, and the device behaves as a standard Bragg grating. For a plasmon resonance at a longer wavelength than λ_{Bragg} (fig. 3(c)), the imaginary part of the refractive index dominates, and the transmission curve corresponds to a Bragg grating modulated by losses [17]. Fig. 3(b) represents an intermediate situation.

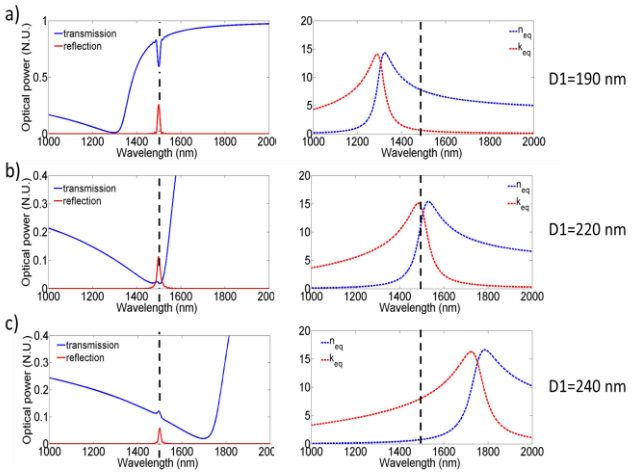

Figure 3: Left column: calculated transmission and reflection spectra of an SOI waveguide with LSP Bragg grating. Right column: real (n_{eq}) and imaginary (k_{eq}) parts of the equivalent layer refractive index. The vertical dashed line shows the spectral position of the Bragg resonance. The long axis of gold ellipsoids is D1 = 190, 220 and 240 nm in a), b) and c), respectively. Their short axis and height are identical in the three cases: D2 = 80 nm, h = 30 nm.

4. FDTD calculations

FDTD calculations were performed to validate the analytical model. Commercial software from Lumerical, FDTD Solutions was used for this purpose. As a precise modeling of > 25 µm long structures (50 gold nanoparticles) with 3 nm accuracy required time-consuming simulations, we therefore limited ourselves to structures comprised of only five nanoparticles, further referred to as "native" Bragg gratings. The spacing between particles was chosen to be 500 nm, close to that measured in fabricated structures (see Section 5). Correspondingly, the grating second order of the grating was calculated to occur at λ =1325 nm. The short axis and the height of the gold ellipsoids were taken to be D2 = 80 nm and h = 30 nm in all the calculations. The length of the ellipsoid axis (D1) varied from 180 to 210 nm.

Figure 4 shows FDTD results for a "native" Bragg grating comprised of five particles with D1 = 180 nm. In this case, the plasmon resonance occurs at a wavelength shorter than the Bragg resonance. In agreement with the theoretical predictions obtained from the analytical model (fig. 3(a)), the waveguide transmission exhibits a minimum at the Bragg wavelength while a maximum is obtained for the waveguide reflection (fig. 4(a)). The field maps show that the propagation of the TE waveguide mode is strongly perturbed by particles. This perturbation is stronger at shorter wavelengths (fig. 4(b)) than at longer wavelengths (fig. 4(d)). At 1326 nm, the two field maximum between neighboring particles (fig. 4(c)) confirms that the Bragg grating is operated in its second order. Interferences between the two counter-propagating waves are well resolved in the first part of the waveguide. A detailed inspection of the field distribution in the central part of the waveguide shows that the field intensity is weak below the particles while it is strong between particles. A very high intensity is also calculated in the very proximity of particles themselves (dotted squares in b), c) and d)). These results justify the approximations used for establishing the coupled mode equations in Section 3.

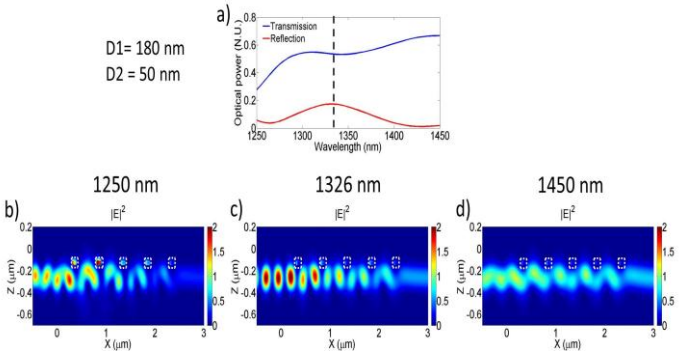

Figure 4: FDTD simulations of a "native" LSP Bragg grating consisting of 5 gold ellipsoids with D1=180 nm, D2 = 50 nm and h = 30 nm. a): waveguide transmission and reflection spectra calculated around the Bragg wavelength (~1326 nm). b), c) and d): mapping of the field intensity $|E|^2$ along a longitudinal waveguide cross-section for λ = 1250, 1326 and 1450 nm, respectively. White dotted squares indicate the positions of the particles.

Figure 5 shows FDTD calculations for D1=190 nm. The plasmon resonance wavelength coincides with the Bragg wavelength in this case. In agreement with predictions from the analytical model (fig. 3(b)), a transmission peak is now observed at the Bragg resonance (fig. 5(a)). The calculated field maps (figs. 5(b, c, d)) are similar to those in fig. 4.

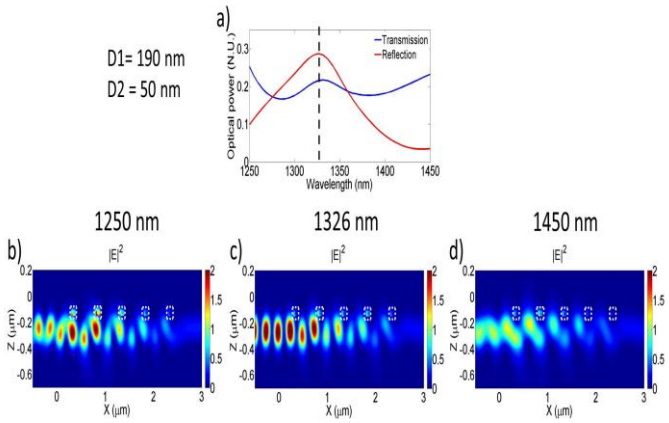

Figure 5: Same as fig. 4 except for D1 = 190 nm

For gold ellipsoids with a long axis D1 = 210 nm (fig. 6), the plasmon resonance is shifted to the long wavelength side of the Bragg resonance. This is again in agreement with the results of the analytical model (fig. 3(c)), the waveguide transmission spectrum exhibits a small peak near the Bragg resonance. The exact location of this peak also depends on the shape of the plasmon absorption curve. The calculated field maps (figs. 6(b, c, d)) are similar to those of fig. 4.

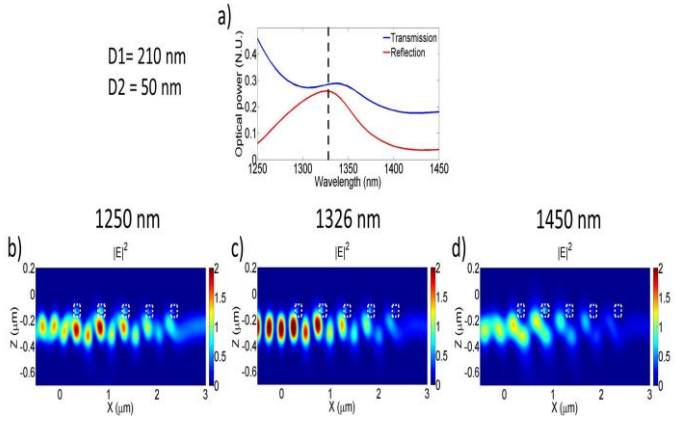

Figure 6: Same as fig. 4 except for D1 = 210 nm.

5. Experiments

Three series of LSP Bragg gratings as schematically shown in fig. 1 were fabricated on single-mode silicon (Si) ridge waveguides having 500 × 220 nm^2 cross-sectional area. All gratings were composed of 50 gold ellipsoids periodically spaced ~ 510 nm apart (fig. 7). The main difference between the three series of gratings was the size of ellipsoids. The long axis and short axis were respectively: D1 = 169 ± 5nm; D2 = 57 ± 5nm (fig. 7(a)), D1 = 181 ± 5nm; D2 = 50 ± 5nm (fig. 7(b)) and D1 = 211 ± 5nm; D2 = 59 ± 5nm (fig. 7(c)). Gold nanoparticles were fabricated on top of the Si waveguides using electron-beam lithography followed by a lift-off process. A 30 nm gold layer was deposited by electron-beam evaporation. A 1 nm titanium (Ti) adhesion layer was deposited prior to the deposition of gold. A Drude model was used to fit the ellipsometric measurements of deposited gold layers. Accurate dispersion data of gold obtained in this way were further used in the analytical model as well as in FDTD simulations.

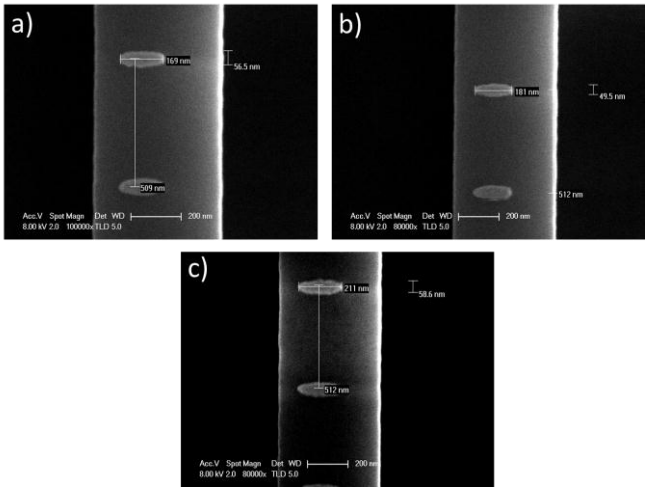

Figure 7: Scanning Electron Microscope (SEM) images of nanoparticles for the three series of fabricated LSP Bragg gratings. The particle sizes are different in the three cases.

The waveguide transmission spectra were measured by injecting a polarized light to the butt facet of the Si waveguide using a lensed polarization maintaining fiber. A cw tunable laser with polarization set to TE was used as the light source. A × 20 objective with 0.35 numerical aperture was used to collect the transmitted light at the waveguide output. The collected light was then detected with a power meter. Normalization of transmission measurements was achieved using a reference waveguide without MNP. The input light was scanned in steps of 1 nm over the 1260-1630 nm range. Figure 8 shows a comparison between experimental results and theoretical results from the

analytical model. "Noise" on the experimental curves is due to Fabry-Perot oscillations caused by reflections at the waveguide ends. For structures a) and b), the LSP resonance occurs at a lower wavelength than the second-order Bragg resonance near 1320 nm. Transmission dips are then experimentally observed at the Bragg resonance in agreement with the predictions of the analytical model (figs. 5(a) and (b)). For gold particles with larger size (fig. 8(c)), the LSP resonance occurs at a longer wavelength than the Bragg resonance. A weak transmission peak is observed in this case as in fig. 5(c). In the three cases a), b) and c), the plasmon linewidth is broader than predicted theoretically. This difference is mainly explained by the quasi-static approximation used in the analytical model. Indeed, radiative losses of metallic dipoles are neglected with the consequence that the calculated LSP resonance presents a better quality factor than the experimental one. On the other hand, fabrication imperfections and particle size dispersion tend to increase the measured LSP bandwidth. It is finally worthwhile noticing that Fabry-Perot oscillations can be used in conjunction with the Bragg grating resonance to produce narrow transmission peaks with relatively high (near 30dB) rejection ratio (fig. 8(c)).

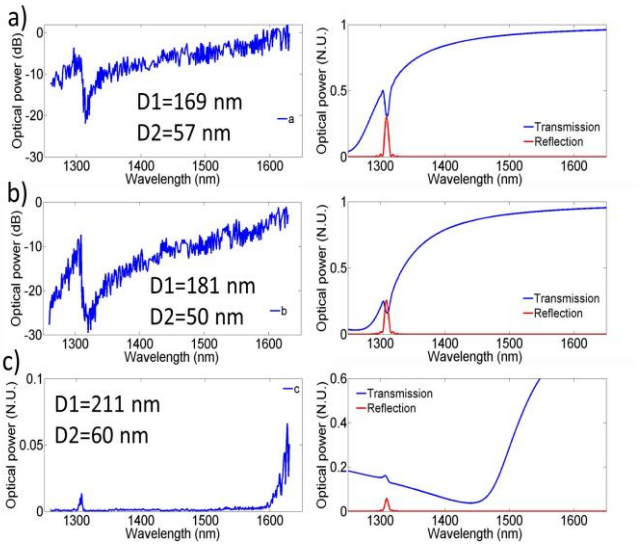

Figure 8: Comparison between experiments and theory. Left column: waveguide transmission spectra measured for fabricated LSP Bragg gratings a), b), and c). In figures a) and b) logarithmic scale is used for better clarity. Right column: theoretical calculations from the analytical model.

6. Conclusion

In this work we have developed the concept of localized surface plasmon Bragg gratings integrated on a dielectric waveguide. We have demonstrated both theoretically and experimentally that different types of transmission responses could be obtained depending on the spectral position of the LSP resonance with respect to the Bragg resonance. As a major result, LSP gratings can be operated either in the refractive index modulation regime or in the loss modulation regime. For a given grating period, the operating regime can be controlled with the size of metallic particles. An analytical model has been developed to qualitatively predict the grating behavior. The model predictions have been verified from FDTD simulations for short gratings with a small number of particles. Although no attempt has been presently made to optimize the LSP Bragg grating performances, we believe that these gratings can find applications in optical filtering and chemical or bio-sensing. Metallic losses in guided optics can be partially compensated for with the use of amplifier waveguide sections.

Acknowledgements

The authors acknowledge R. Colombelli and D. Costantini for useful discussions, C. Delacour and A. Chelnokov for sample preparation. This work has been supported by the Agence Nationale de la Recherche under the PLACIDO N^{o} ANR-08-BLAN-0285-01 project. M. Février recieved financial support from the Region Ile-de-France.

References

[1] W. L. Barnes, A. Dereux and T. W. Ebbesen, Nature, 424, 824, (2003).
[2] M. A. Noginov et al., Nature, 460, 1110, (2009).
[3] D. K. Lim, K. S. Jeon, H. M. Kim, J. M. Nam and Y. D.Suh, Nature Mater. 9, 60, (2010).
[4] S. M. Nie and S. R. Emery, Science. 275, 1102, (1997).
[5] C. Huang et al., Biomed Microdevices. 11, 839, (2009).
[6] M. Quinten, A. Leitner, J. R Krenn and F. R. Aussenegg, Opt. Lett. 23, 1331, (1999).
[7] J. R Krenn et al., Phys. Rev. Lett. 82, 2890, (1999).
[8] M. Fevrier et al., Nano letters. 12, 1032, (2012).
[9] S. L. Zou, N. Janel and G. C. Schatz, J. Chem. Phys. 120, 10871, (2004).
[10] Y. Z. Chu, E. Schonbrun, T. Yang and K. B. Crozier, Appl. Phys. Lett. 93, 181108, (2008).
[11] V. G. Kravets, F. Schedin, and A. N. Grigorenko, Phys. Rev. Lett. 101, 087403, (2008).
[12] R. Quidant, C. Girard, J. C. Weeber, and A. Dereux, Phys. Rev. B. 69, 085407, (2004).
[13] W. Zhou and T. W. Odom, Nature Nanotech. 6, 423, (2011).
[14] Y. Uchio, M. Shimojo, K. Furuya and K. Kajikawa, J. Phys. Chem. C, 114, 4816, (2010).
[15] S. Zhang, D. A. Genov, Y. Wang, M. Liu, and X. Zhang, Phys. Rev. Lett. 101, 047401, (2008).
[16] R. D Kekapture, E. S. Barnard, W. Cai, and M. Brongersma, Phys. Rev. Lett. 104, 243902, (2010).
[17] A. Yariv and P. Yeh. Photonics optical electronics in modern communications, sixth edition, Oxford University press, 2005.
[18] E. Lidorikis, S. Egusa and J. D. Joannopoulos, J. Appl. Phys. 101, 054304, (2007).
[19] T. Yamaguchi, S. Yoshida, and A. Kinbara, Thin Solid Film. 21, 173, 1974.
[20] C. F. Bohren and D. R. Huffman, Wiley : New York, (1983).
[21] J. Jackson. Classical Electrodynamics. Wiley : New York, (1999).